Proceedings of the 6th International Conference on Ship and Offshore Technology
ICSOT 2019
November 7-8, 2019, IIT Kharagpur, India

ICSOT INDIA 2019-06

ANALYSIS OF FORCES AND FLOW FEATURES OF A WAVY CYLINDER AT LOW REYNOLDS NUMBER

Arijit Pradhan
IIT(ISM) Dhanbad
Dhanbad, Jharkhand, 826004
India
arijit575@gmail.com

Ravi Chaithanya Mysa
Singapore University of
Technology and Design
Singapore, 487372
Singapore
ravichaithanya.mysa@gmail.com

Subhankar Sen
IIT(ISM) Dhanbad
Dhanbad, Jharkhand, 826004
India
subhankars@mail.com

ABSTRACT

The attempt to use wavy cylinders in the offshore industry is bio-inspired from the vibrissa of the harbor seal vibrissa. The ability to detect the prey in worse conditions by the seal vibrissa is due to the sensitivity of the wavy cylinder to the wakes of the prey. A clear understanding of the flow physics of the stationary wavy cylinder and its vortex-induced vibrations in a uniform flow, as well as the non-uniform flow, has to be studied in detail for venturing into the applications in off-shore industry. In the present numerical study, the unsteady flow physics and the force variation due to the wavy nature of the stationary cylinder is studied in detail. The Reynolds number considered for the study is 100. The geometry of the cylinder is parametrized by the wavelength λ, wave amplitude a, and mean diameter, D_m of the cylinder sinusoidal curve. The Results are presented for the non-dimensional parameter λ/D_m varying between 3.5 and 9. The wave amplitude along the span of the cylinder for the numerical investigation has been fixed to 0.1. A detailed analysis based on the pressure variation along the span of the wavy cylinder and it's near flow features is done and an explanation is provided for the source of force in the paper.

INTRODUCTION

Vortex-induced vibration (VIV) of bluff bodies finds application in off-shore, tall buildings, power lines, bridges, chimneys, and energy conversion equipment. The vortex shedding from these vortices generates oscillatory forces on the bluff body. The control of vortex shedding for suppression of VIV and extracting energy is a challenging issue. Lam and Lin [1] investigated a series of wavy cylinder with different combinations of wave amplitude and wavelength to study the effect of drag force over the cylinder surface at low Reynolds number. It has been shown that the free shear layers from the wavy cylinder are difficult to roll up to vortex and it causes an increase in wake formation length of the wavy cylinder. Yoon et. al [2] have studied the reduction in drag coefficient and lift coefficient on an asymmetric wavy cylinder at Reynolds number 3000. They have shown that the length of vortex formation for an asymmetric wavy cylinder is longer than that of a symmetric wavy cylinder. And there is a significant reduction in drag and lift coefficient than the symmetric cylinder. Darekar and Sherwin [3] have numerically investigated flow past square wavy cylinder. The introduced waviness at Reynolds number 100 results in stabilization of near wake compared to fully developed shedding in a straight square cylinder. It has been found out that an increase in wave amplitude results in the emergence of hairpin vortices from the near wake region. The introduction of waviness at a wavelength close to the mode A wavelength leads to the suppression of the Karmann street at a minimal waviness amplitude. Ahmed et. al [4] have experimentally studied the transverse flow over a set of wavy cylinder with different axial wavelengths. The Presence of spanwise pressure gradients results in three-dimensional separation lines and the formation of streamwise trailing vortex structure near the geometric nodes. They have shown that there is a larger sectional drag coefficient at the geometric nodes than at the geometric saddles.

Lam et. al [5] have done numerous experiments to study the near wake of a wavy cylinder. The crossflow mechanism around the wavy cylinder reveals the average vortex formation length behind a wavy cylinder is longer than that of a circular cylinder, which effectively reduces the drag and suppresses the vibration. The free shear layers shed from the points near the saddles extend along the spanwise direction, while the shear layer near the nodes contract. Lam et. al [6] conducted wind tunnel experiments to study the effects of the surface waviness of wavy(varicose) cylinders. The experiments are conducted with Reynolds number between $2.0x10^4$ and $5.0x10^4$ and free stream turbulence intensity less than 0.2%. It has been concluded from the experiment that drag reduction of up to 20% can be achieved. The spectral analysis of both hot-wire and load cell signal shows the Strouhal number of a wavy cylinder and corresponding circular cylinder remains the same. Vibrations of a thin and flexible cylinder under nominally constant towing conditions are studied by Dowling [7]. They have shown that the displacement near to critical points depends on normal and tangential drag coefficient C_N and C_T. Kim and Yoon [8] have studied the effect of angle of

attack on harbor seal vibrissa shaped cylinder on flow characteristics at Reynolds number 500. They have shown that there exist longer shear layers for the said cylinder than elliptic cylinder at smaller angle of attack. But, with increase in angle of attack, the flow contours become similar to that of an elliptic cylinder.

In the present work, numerical simulation has been carried out to study the effect of waviness on the net fluid force exerted on the cylinder. We are intending to study the detailed analysis on the origin of forces in this work. In later part of the work, the vortex-induced vibration (VIV) pattern and its cause, has been analyzed for a wavy cylinder. A series of different values of non-dimensional parameter, λ/D_m has been taken into account. The ratio of wave amplitude to mean cylinder diameter, a/D_m is fixed at 0.1. The whole study has been carried out at Reynolds number Re, 100. In the next section, the mathematical concept behind the numerical simulation has been explained.

MATHEMATICAL MODELING

The governing Navier-Stokes equation for the unsteady incompressible flow in the Arbitrary Lagrangian Eulerian (ALE) approach is described by:

$$\nabla . \boldsymbol{U} = \boldsymbol{0} \tag{1}$$

$$\frac{\partial \mathbf{U}}{\partial \mathbf{t}} + \nabla . \left((\boldsymbol{U} - \cup \boldsymbol{g}) \boldsymbol{U} \right) = -\nabla \boldsymbol{p} + \nabla . (\nu \nabla \boldsymbol{U}) \tag{2}$$

Where **U**, p, $\mathbf{U_g}$ and ν represent the fluid velocity, pressure, velocity of the moving mesh and kinematic viscosity of the fluid respectively. The momentum equation is discretized using an implicit one step Euler discretization in time,

$$\mathrm{a_p U_p^{n+1}} = \sum_f \mathrm{a_f} U_f^{n+1} = -\nabla p^n + \frac{U^n}{dt} \tag{3}$$

The above equations are solved over multiple outer and inner corrector steps for forwarding the solution over one time step in the openFoam solver *pimpleDymFoam* [5]. For each outer corrector, the non-linear term $(\mathbf{U}\text{-}\mathbf{U_g})\mathbf{U}$ is linearized such that the term $(\mathbf{U}\text{-}\mathbf{U_g})$ appears as relative face flux at a previous outer corrector. The term a_p and a_f contain the coefficients of discretization, which also includes the relative face flux.

The inner correctors follow the Pressure Implicit with Splitting of Operators (PISO) algorithm. This can be achieved by casting the momentum equation in such a way that it enforces a zero discrete at the following inner correctors as follows:

$$\mathbf{U_f^{n+1}} = \frac{\boldsymbol{H}(\mathbf{U^{n+1}})}{a_{p,f}} - \frac{\nabla p_f^{n+1}}{a_{p,f}} \tag{4}$$

Where,

$$\boldsymbol{H} = \sum_f \mathrm{a_f} U_f^{n+1} + \frac{\boldsymbol{U^n}}{dt} \tag{5}$$

The Poisson equation for pressure can be obtained by taking the discrete divergence of equation - (4).

$$\sum_f \frac{\nabla p_f}{a_{p,f}} . \boldsymbol{S} = \sum_f \frac{\boldsymbol{H}}{a_{p,f}} . \boldsymbol{S} \tag{6}$$

Where **S** is the area vector of the given face. *pimpleDymFoam* is developed by merging the PISO and SIMPLE algorithms for a dynamic mesh case. The pressure is relaxed and end of each inner corrector step in the PISO algorithm, which gives rise to the SIMPLE algorithm. The number of outer correctors are determined through a residual criteria, whereas the number of inner correctors is fixed to 2-3 for this work.

The different non-dimensional parameters used in this study are mass ratio m^*, Reynolds number *Re*, reduced velocity U_r, and damping ratio ς are defined as follows:

$$m^* = \frac{m}{m_f}, \qquad Re = \frac{U_\infty D_m}{\nu}, \qquad U_r = \frac{U_\infty}{f_N D_m}, \qquad \zeta = \frac{c}{\sqrt{km}} \tag{7}$$

Where *m* is mass of the bluff body, m_f is the mass of the fluid displaced by the bluff body, *c* is the damping coefficient, and *k* being the stiffness constant for an equivalent spring-mass-damper system. U_∞ and D_m are the free stream speed and mean diameter of the cylinder respectively. The natural frequency of the bluff body is defined as $f_N = (1/2\pi)\sqrt{(k/m)}$. The drag coefficient C_D is defined as:

$$C_D = \frac{1}{\frac{1}{2}\rho U^2 D} \int_S \left(\left(-p\mathbf{I} + \mu \left(\nabla \mathbf{U} + (\nabla \mathbf{U})^{\mathbf{T}} \right) \right) . \mathbf{n} \right) . \mathbf{n_x} dS \tag{8}$$

$$\mathrm{cd_{avg}} = \frac{\int_0^T cd(t)dt}{\int_0^T dt} \tag{9}$$

Where **S** is the surface area of the wavy cylinder, μ and ρ being the dynamic viscosity and density of fluid respectively, **n** is the unit normal vector to the plane and **I** is the identity matrix. The lift coefficient due to pressure force C_{Lp} and lift coefficient due to viscous force $C_{L\mu}$ are defined as:

$$C_L = \frac{1}{\frac{1}{2}\rho U^2 D} \int_S \left(\left(-p\mathbf{I} + \mu \left(\nabla \mathbf{U} + (\nabla \mathbf{U})^{\mathbf{T}} \right) \right) . \mathbf{n} \right) . \mathbf{n_y} dS \tag{10}$$

$$Cl_{rms} = \sqrt{\frac{\int_0^T [cl(t)]^2 dt}{\int_0^T dt}} \tag{11}$$

$$C_{Lp} = \frac{1}{\frac{1}{2}\rho U^2 D} \int_S \left(\left(-p\mathbf{I}.\mathbf{n} \right) . \mathbf{n_y} dS \right) \tag{12}$$

$$C_{L\mu} = \frac{1}{\frac{1}{2}\rho U^2 D} \int_S \mu \left(\left(\nabla \mathbf{U} + (\nabla \mathbf{U})^{\mathbf{T}} \right) . \mathbf{n} \right) . \mathbf{n_y} dS \tag{13}$$

PROBLEM DESCRIPTION

A series of wavy cylinders with different combination of parameters has been studied in this work. The sinusoidal function for generating the wavy surface of the cylinder is being defined as follows:

$$D = D_m + 2a\cos\left(\frac{2\pi z}{\lambda}\right) \quad (14)$$

Figure 1(a) shows the geometric parameters of the wavy cylinder. Figure 1(b) depicts the schematic diagram of the flow domain with different boundary conditions. The base of the wavy cylinder is circular. The wave amplitude is denoted by 'a' and the wave length is denoted by λ.

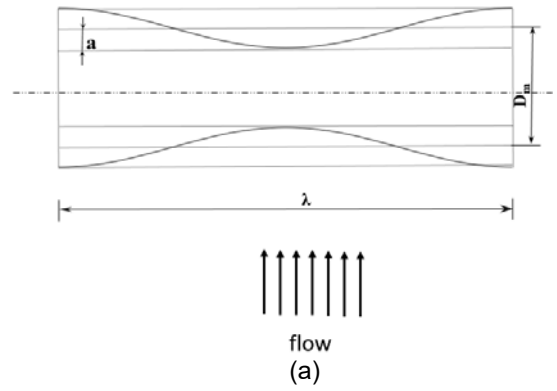

(a)

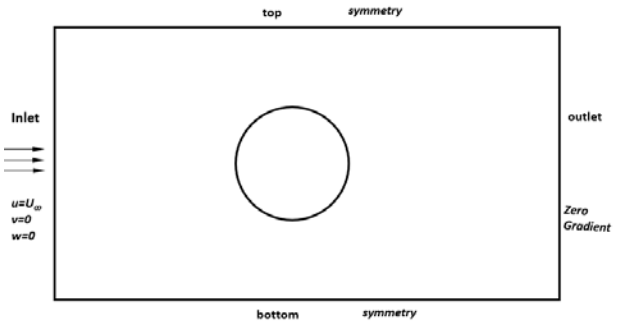

(b)

Figure1: SCHEMATIC REPRESENTATION (a). GEOMETRIC PARAMEMTERS OF WAVY CYLINDER (b). COMPUTATIONAL DOMAIN

VERIFICATION AND MESH CONVERGENCE

The mesh convergence study has been carried out for two test cases with λ/D_m=3.5. The results for the comparison has been presented in Table-1. The mesh with size near to 700,000 gives converged results. Thus, this grid size has been chosen for further computation purpose.

Table 1. MESH CONVERGENCE STUDY

Case	Number of Cells	Cd_{avg}	%Change in Cd_{avg}
1	1381527	1.3395	0.1621
2	727982	1.3416	

The validity of the formulated numerical method is need to be checked before further discussion. This section presents the mesh convergence test and validity of the computational data with reference to the work of Lam et. al [1]. The average drag coefficient, Cd_{avg} has been compared for different values of λ/D_m. Table 2 shows the comparison of Cd_{avg} with the results from the work of Lam et. al [1]. From the table it has been observed that the % change is very small, thus validates our numerical method.

Table 2. VALIDATION OF THE NUMERICAL METHOD

λ/D_m	$Cd_{avg,\ Reference}$	$Cd_{avg,\ computation}$	%Change in Cd_{avg}
3.5	1.3297	1.3188	0.8139
4.0	1.2950	1.2797	1.1816
5.4	1.1599	1.1489	0.9522
5.8	1.1411	1.1411	0.4085
9.0	1.1391	1.1391	8.0214

RESULTS AND DISCUSSION

In this text the behavior of wavy cylinder has been studied with carrying several numerical computations at Re = 100. To study the effects of forces due to the curvature of wavy cylinder, the time dependency of coefficient of drag and lift need to be considered for different values of λ/D_m. For the

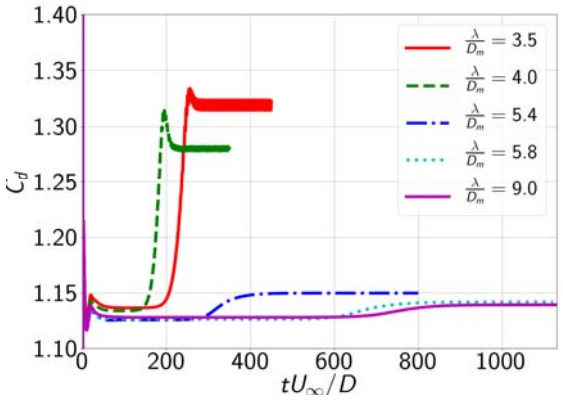

(a)

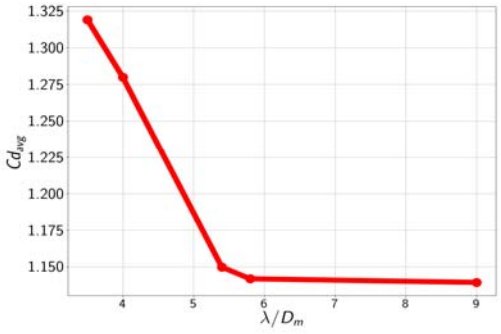

(b)

Figure 2: (a). TIME HISTORY VARIATION OF DRAG COEFFICIENT (b) VARIATION OF MEAN DRAG COEFFICIENT WITH DIFFERENT VALUES OF λ/D_m.

current study, the value of a/D_m has been fixed at 0.1. Figure 2 shows the variation of drag coefficient, C_d with time and the geometrical parameter, λ/D_m. As the value of λ/D_m increases, the value of Cd_{avg}, decreases. The graph asymptotically approaches 0.12 as we increases the value of λ/D_m. For circular cylinder the value of drag coefficient is near to 1.33. Thus adding waviness to a circular cylinder reduces the drag force.

Figure 3 shows the variation of lift coefficient, C_l. The RMS value of lift coefficient varies in a similar fashion as Cd varies with λ/D_m. As the value of λ/D_m increases, the root mean square value of lift coefficient decreases. Figure 2 - 3 shows that the waviness decreases the net fluid force exerted on the bluff body.

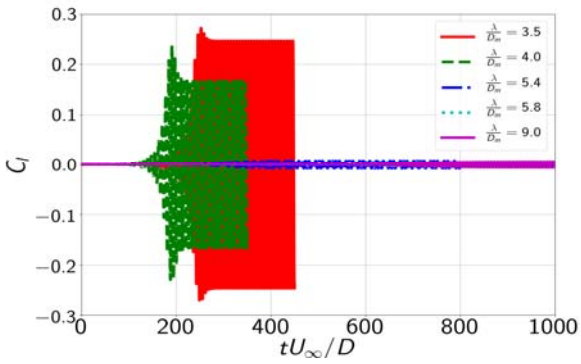

(a)

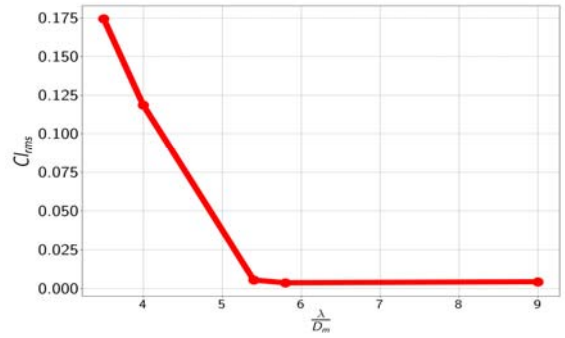

(b)

Figure 3: (a) TIME HISTORY VARIATION OF LIFT COEFFICIENT (b). VARIATION OF LIFT COEFFICIENT WITH DIFFERENT VALUES OF λ/D_m

Figure 4 shows the vorticity contours of wavy cylinder at three different sections for different values of λ/D_m. For the purpose of analysis, nodal plane $z/\lambda=0$, saddle plane $z/\lambda=0.5$ and the mid plane of these two cross sections $z/\lambda=0.25$ has been chosen. Here it's worth mentioning that the wavy cylinder is symmetrical about the mid plane, i.e., $z/\lambda=0.5$. Thus the observed parameters also do behave symmetrically with respect to the mid plane. As the value of λ/D_m increases, it is being observed that the vortex sheet do not roll to form vortex, which causes suppression of vortex shedding near to the cylinder. For λ/D_m =9.0, the vortex formation is least, whereas for λ/D_m=3.5, vortex shedding do occur. This facilitates the previous observation that with increase in λ/D_m, there is a reduction in the net fluid forces over the cylinder. Now, for each λ/D_m, there is a difference in vorticity contours for the three shown planes. Thus instead of two-dimensional vortices as in the case of a circular cylinder, here the vortex contour pattern is three dimensional in nature. Due to the three dimensional nature of the vortex formation pattern, the vortex

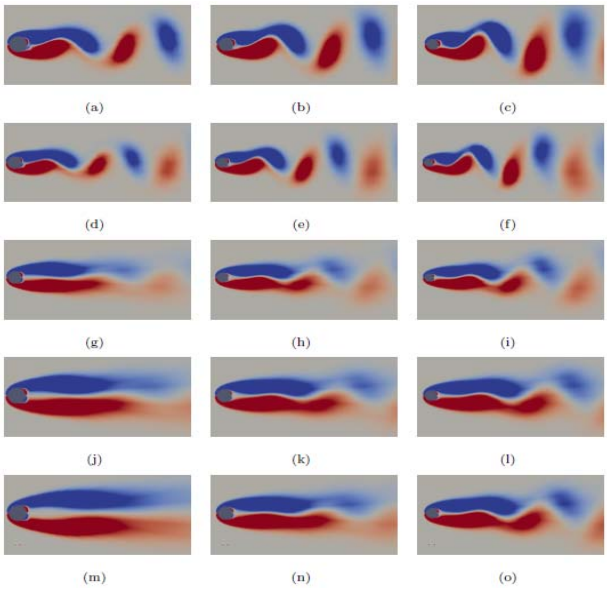

Figure 4. VORTICITY CONTOURS AT THE INSTANT OF TIME WHEN C_{lp} is MAXIMUM. 1ST COLOUMN $z/\lambda=0$, 2nd COLOUMN $z/\lambda=0.25$, 3rd COLOUMN $z/\lambda=0.5$ (a)-(c) λ/D_m =3.5, (d)-(f) λ/D_m =4.0, (g)-(i) λ/D_m =5.4, (j)-(l) λ/D_m =5.8, (m)-(o) λ/D_m =9.0

sheet finds it difficult to roll into a full vortex. As the vortex sheet pattern on each plane is different, thus it does not roll to form vortex in the near wake region. Thus the fluctuating forces are absent or very low in case of wavy cylinder at higher value of λ/D_m.

PRESSURE DISTRIBUTION

To understand the nature of fluid forces around the periphery of the cylinder, we will now look at the coefficient of pressure distribution, C_p on the cylinder. The coefficient of pressure, C_p is mathematically defined as $C_p = 2p/\rho U_\infty^2$. Figure 5 shows three graphs showing the variation of C_p with respect to θ measured anticlockwise. The pressure coefficient variation with respect to theta on $z/\lambda=0$ plane gets superimposed on that of z/λ =1 plane. And similarly the pressure variation with respect to theta on z/λ =0.25 plane and z/λ =0.75 plane overlap each other. Thus it's graphically verifies our previous observation that the properties are symmetric about the mid plane i.e., z/λ =0.5 plane.

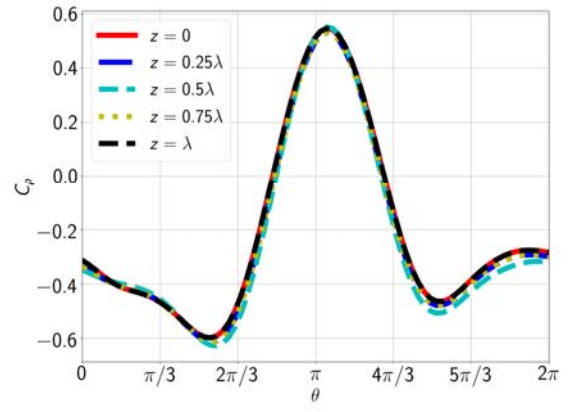

(a)

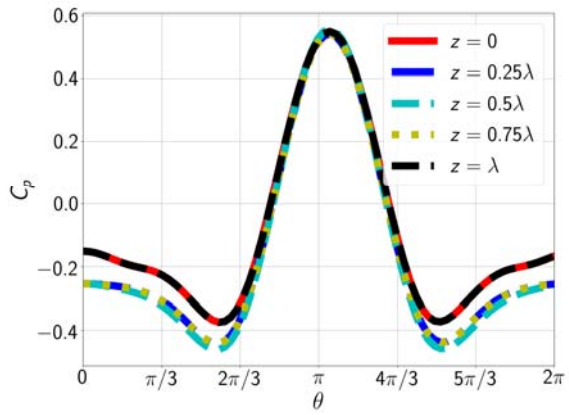

(b)

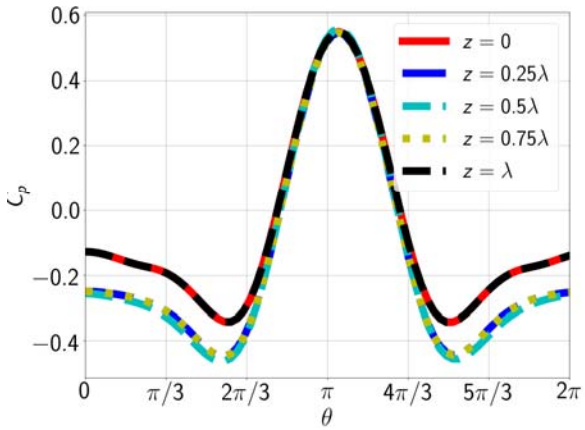

(c)

Figure 5: C_p-θ VARIATION ACROSS 5 PLANES i.e., z/λ=0, 0.25, 0.5, 0.75, 1.0 FOR λ/D_m= (a).3.5 (b). 5.8 (c). 9.0

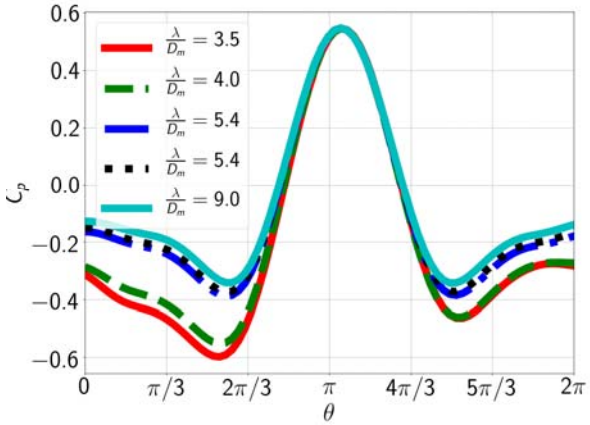

(a)

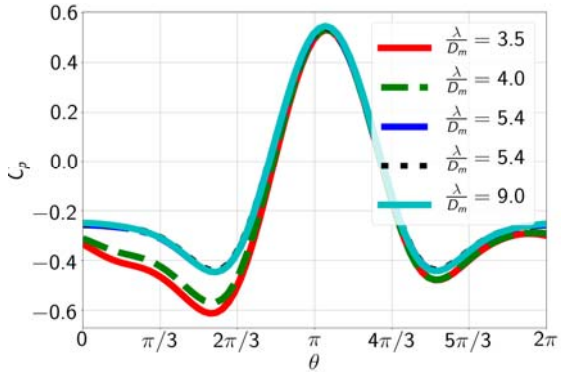

(b)

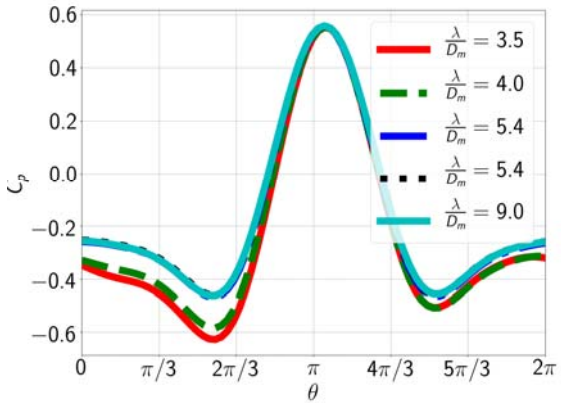

(c)

Figure 6: C_p-θ VARIATION AT THE INSTANT OF $C_{l,pmax}$ FOR DIFFERENT VALUES OF λ/D_m FOR z/λ = (a). 0 (b). 0.25 (c). 0.5

At the instant when the lift force, $C_{l,p}$ is maximum, then the suction pressure on top part of the cylinder, $0 \leq \theta \leq \pi$ is more than the bottom part of the cylinder. Thus the top region is designated as the high suction pressure region, where as the bottom portion is called as the low suction pressure region. This designations get reversed if we will talk about the C_p-θ plot at the instant when $C_{l,p}$ is minimum. This is depicted in figure 6. Here, the stagnation point lies on the low suction region, irrespective of the value of λ/D_m The stagnation point for a given normalized plane remain constant for different values of the parameter λ/D_m. The suction pressure is maximum for λ/D_m =3.5. Since for λ/D_m=3.5, rolling of vortex occurs, which causes maximum suction pressure for lower value of λ/D_m. As λ/D_m increases, the value of suction pressure decreases, which is coherent with our previous observation. For z/λ=0 plane the variation in suction pressure is more compared to the saddle plane i.e, z/λ=0.5.

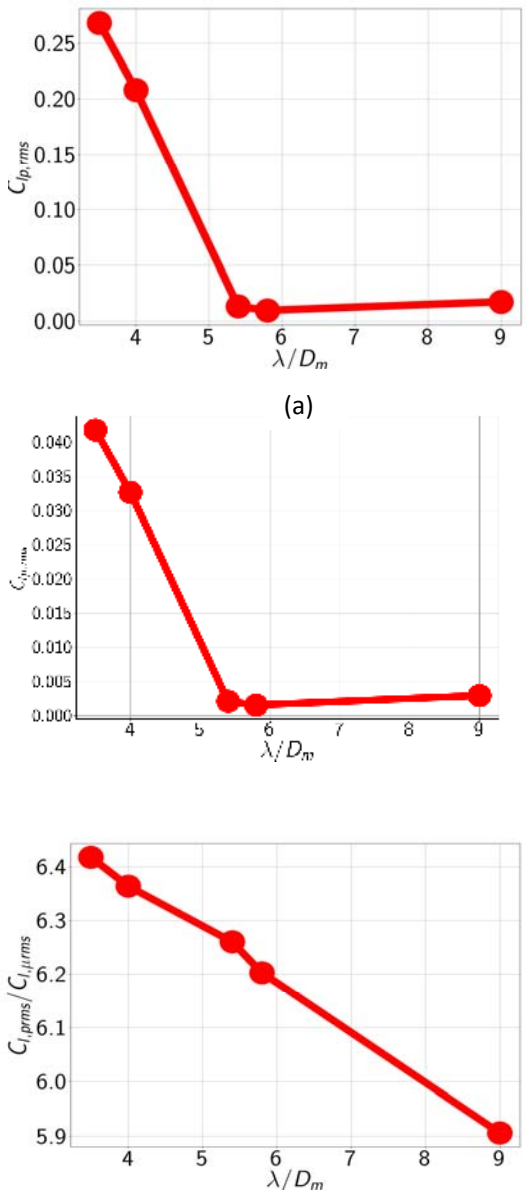

Figure 7: (a). VARIATION OF C_{lp} FOR DIFFERENT VALUES OF λ/D_m (b). VARIATION OF $C_{l\mu}$ FOR DIFFERENT VALUES OF λ/D_m (c). VARIATION OF $C_{lp,\,rms}/\,C_{l\mu,\,rms}$ FOR DIFFERENT VALUES OF λ/D_m

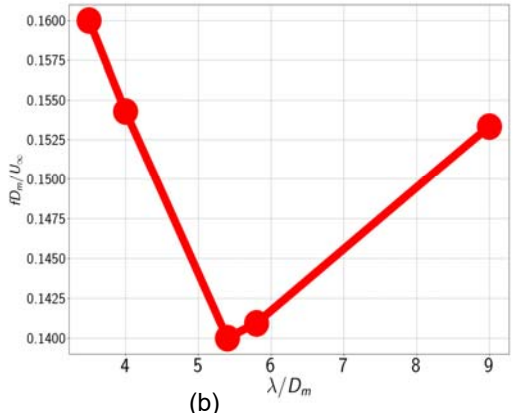

Figure 8: (a) VARIATION OF LIFT COEFFICIENT IN FREQUENCY DOMAIN (b). VARIATION OF FREQUENCY RATIO WITH λ/D_m

For clear understanding of the effect of transverse force on the cylinder, the lift force coefficient has been decomposed into two parts. The two parts are lift force due to pressure, $C_{l,p}$ and lift force due to viscosity, $C_{l,\mu}$. The root mean square value of lift coefficient due to pressure and viscosity decrease steadily with λ/D_m, conforming to our previous observation. Figure 7 (a)-(b) shows this behavior. Figure 7(c), shows that the effect of $C_{l,p}$ per unit $C_{l,\mu}$ decreases with λ/D_m. The effect of $C_{l,\mu}$ component increases with λ/D_m.

Figure 8 shows the contribution of different frequency components in lift coefficient. The maximum value of normalized frequency for λ/D_m=3.5 to 9.0 is 0.16, which is very low compared to circular cylinder. Figure 8(b) shows that the frequency component decreases with λ/D_m upto λ/D_m =5.4, and then it increases.

VIV OF WAVY CYLINDER

In this section, we will briefly discuss about the VIV of the wavy cylinder. The results of wavy cylinder with geometrical parameter, λ/D_m=5.8 at Re=100 and m^*=10 is being compared with the results from the work of Leontini et. al [10] for a circular cylinder at Re=200 and m^*=10. The behavior of circular cylinder at Re=200 will not differ much from that of Re=100. Thus the works of Leontini et. al[10] will serve our purpose. Figure 9(a) shows the variation of frequency ratio, f/f_N with respect to U_r. The lock-in region for a wavy cylinder

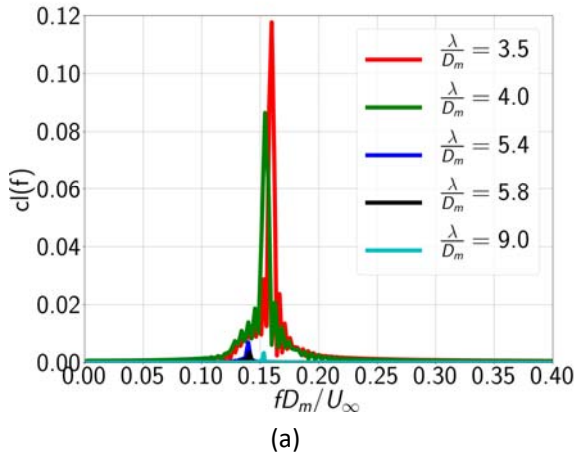

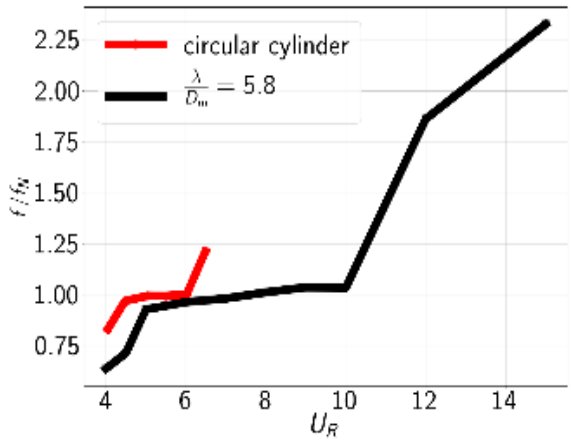

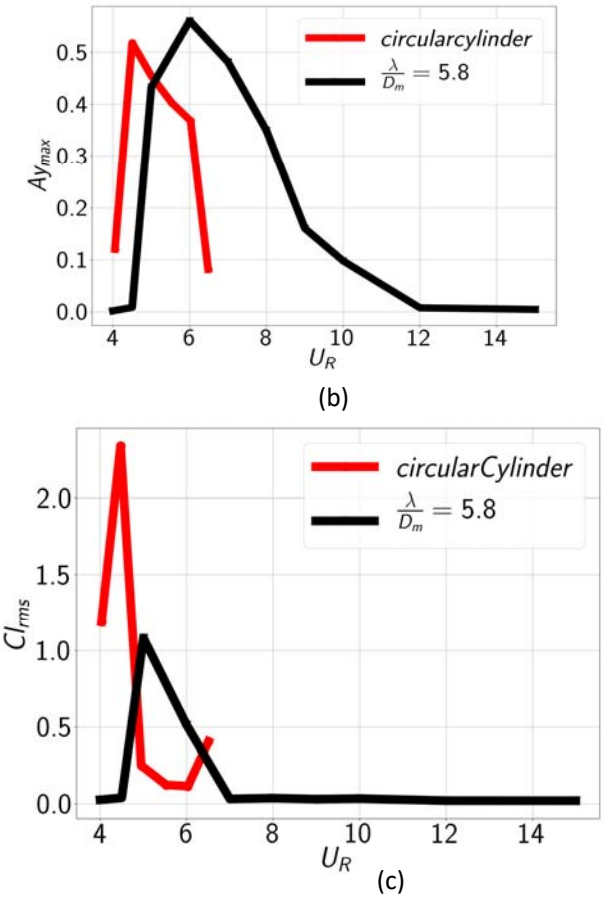

Figure 9: COMPARISON OF PROPERTIES OF WAVY CYLINDER WITH λ/D_m =5.8, Re=100, m^*=10 WITH CIRCULAR CYLINDER DATA FROM LEONTINI et. al HAVING Re=200, m^*=10 (a). VARIATION OF FREQUENCY RATIO f/f_N WITH U_r (b). VARIATION OF $A_{y,max}$ WITH U_r (c). VARIATION OF $C_{l,rms}$ WITH U_r

with λ/D_m =5.8 will be between U_r=4.5 to U_r=10.0. But, for circular cylinder, it will lie between U_r=4.5 to U_r=6.0. The lock-in region for a wavy cylinder is larger than that of the circular cylinder. Figure 9(b) shows the variation of $A_{y,max}$ with respect to U_r. $A_{y,max}$ is calculated by using the formula $A_{y,max}=\sqrt{2}A_{y,rms}$. Here, the maximum value of amplitude, $A_{y,max}$ for both circular cylinder as well as wavy cylinder is near to 0.5. For both circular cylinder and the wavy cylinder, the amplitude curve follows the same pattern i.e., increasing up to a particular point and then decreasing steadily. The critical point for the wavy cylinder is at U_r=6, whereas for circular cylinder, it is Ur=4.5. Figure 9(c) shows the variation of Cl_{rms} with respect to U_r. For circular cylinder the root mean square value of lift coefficient is generally higher than that of a wavy cylinder with λ/D_m =5.8. The maximum value of Cl_{rms} do occur at Ur=4.5 for the circular cylinder, but for the wavy cylinder, it do occur at U_r=5.0.

CONCLUSION

In the present work the flow features of a wavy cylinder at Reynolds number, Re=100 has been studied for stationary as well as VIV cases. A series of wavy cylinder has been taken for numerical simulation with λ/D_m from 3.5 to 9.0. The ratio of wave amplitude to the mean diameter of the wavy cylinder, a/D_m is 0.1. The VIV of wavy cylinder has been compared with the works of Leontini et. al [10]. It has been observed that with increasing λ/D_m, the net fluid force on the cylinder decreases. The three-dimensional nature of the vortex formation pattern makes it difficult for the vortex to roll. So, with increase in the value of λ/D_m, the tendency of vortex to roll decreases and so is the vortex shedding. The pressure distribution around the cylinder periphery depicts the same observation. It has been observed that for a wavy cylinder with λ/D_m =5.8, the lock-in region is larger compared to a circular cylinder. The transverse force on a wavy cylinder is significantly lower than the circular cylinder.

REFERENCES

[1] K. Lam, Y. F. Lin, Drag force control of flow over wavy cylinders at low reynolds number Journal of Mechanical Science and Technology 21 (9) (2007) 1331. Doi: 10.1007/BF03177417 https://doi.org/10.1007/BF03177417

[2] H. S. Yoon, H. Shin, H. Kim, Asymmetric disturbance effect on the flow over a wavy cylinder at a subcritical Reynolds number, Physics of Fluids 29 (9) (2017) 095102 doi:10.1063/1. https://doi.org/10.1063/1.5001968

[3] R. M. DAREKAR, S.J. SHERWIN, Flow past a square-section cylinder with a wavy stagnation face, Journal of Fluid Mechanics 426 (2001) 263-295, doi:10.1017/S0022112000002299

[4] A. Ahmed, B. Bays-Muchmore, Transverse flow over a wavy cylinder, Physics of Fluids A: Fluid Dynamics 4 (9) (1992) 1959-1967, doi: 10.1063/1.858365, https://doi.org/10.1063/1.858365

[5] K. Lam, F. H. Wang, R. M. C. So, Three-dimensional nature of vortices in the near wake of a wavy cylinder, Journal of Fluids and Structures, 19 (2004) 815-833, doi: 10.1016/j.jfluidstructs.2004.04.004, http://adsabs.harvard.edu/abs/2004JFS....19..815L

[6] K. Lam, F.Wang, J. Li, R. So, Experimental investigation of the mean and fluctuating forces of wavy (varicose) cylinders in a cross-flow, Journal of Fluids and Structures, 19 (3) (2004) 321-334 doi: https://doi.org/10.1016/j.jfluidstructs.2003.12.010 http://www.sciencedirect.com/science/article/pii/S0889974604000271

[7] A. P. Dowling, The dynamics of towed flexible cylinders Part 1. Neutrally buoyant elements, Journal of Fluid Mechanics 187 (1988) 507-532. doi: 10.1017/S0022112088000540

[8] H. Kim, H. S. Yoon, Effect of the orientation of the harbor seal vibrissa based biomimetic cylinder on hydrodynamic forces and vortex induced frequency, AIP Advances 7(10) (2017) 105015. doi: 10.1063/1.5008658 https://doi.org/10.1063/1.5008658

[9] H. Jasak, A. Jemcov, Z.Tukovic, OpenFOAM: A C++ library for complex physics simulations

[10] J.S. Leontini, M.C. Thompson, K. Hourigan, The beginning of branching behaviour of vortex-induced vibration during two-dimensional flow, Journal of Fluids and Structures. doi:https://doi.org/10.1016/j.jfluidstructs.2006.04.003 http://www.sciencedirect.com/science/article/pii/S088997460600051X